ISSN (Print) 1226-1750
ISSN (Online) 2233-6656
Journal of Magnetics 20(2), 166-175 (2015) http://dx.doi.org/10.4283/JMAG.2015.20.2.166

Design and Torque Ripple Analysis of Brush-less DC Motor According to Delta Winding Connection

Tae-Yong Lee[1], Myung-Ki Seo[1], Yong-Jae Kim[2], and Sang-Yong Jung[1]*

[1]*Department of Electrical and Computer Engineering, Sungkyunkwan University, Suwon 440-746, Korea*
[2]*Department of Electrical Engineering, Chosun University, Gwangju 501-759, Korea*

(Received 22 January 2015, Received in final form 9 June 2015, Accepted 10 June 2015)

In this study, we describe the design method of a Brush-less DC (BLDC) motor with delta winding connection. After designing delta winding connection model with the 60° flat-top region of the Back Electro-Motive Force (BEMF), an ideal current source analysis and a voltage source analysis, with a 6-step control, were conducted primarily employing Finite Element Method. In addition, as a current controller, we considered the Current Regulator with PI controller using Simulink for the comparison of torque characteristics. When the input current is controlled, the switching regions and reference signals are determined by means of the phase BEMF zero-crossing point. In reality, the input current variation depends on the inductance as well as input voltage, and it causes a torque ripple after all. Therefore, each control method considered in this research showed different torque ripple results. Based on the comparison, the causes of the torque ripple have been verified in detail.

Keywords : brush-less DC motor, delta winding connection, ideal current source analysis, PI control, 6-step voltage source analysis, torque ripple

1. Introduction

Brush-less DC (BLDC) motors exhibit outstanding performances in terms of their efficiency, power density, and speed ranges [1, 2]. Due to these characteristics and their reasonable cost, they are applied in various industrial fields, such as vehicles, home appliances, and servo motors with a simple operating system [3].

BLDC motor uses switching devices instead of brush and commutator. Also, it employs an armature system, which consists of a stator with coil, and field system which consists of a permanent magnet attached to a rotor. For this reason, it has the advantages of allowing for greater variation of the structure compared to general DC motors. In other words, it makes it possible to optimize the structure for various purposes, such as size minimization, flattening, and etc. [4-6]. The absence of brush and commutator influences the operating range capability, especially the high speed driving point. Moreover, it is easier to apply cooling system, since coils are located at the stator part, and this alleviates the demagnetization problem of the permanent magnet and improves the current limit condition. Furthermore, BLDC motors have an approximately 15% higher power density than AC type motors, due to the higher Root-Mean-Square (RMS) value of the trapezoidal Back Electro-Motive Force (BEMF) than the sinusoidal BEMF [7].

In principle, there exist two different winding arrangements for BLDC motor, the delta connection and wye connection. Depending on the winding arrangements, the required phase BEMF waveforms are different, although their basic wave forms show trapezoidal. In case of the delta winding connection, the required flat-top region of the phase-BEMF is 60°, while in case of the wye winding connection, a 120° flat-top region is required. These BEMF characteristics cannot be obtained through the winding arrangement automatically. Thus, the BLDC motor must be designed with respect to the winding pitch and pole-arc according to the winding arrangement type to satisfy the specific form of the phase BEMF [8]. After fulfilling the BEMF condition, the input current should be controlled in accordance with the BEMF for a constant torque.

In this research, we described the design method of

*Corresponding author: Tel: +82-31-290-5811
Fax: +82-31-299-4918, e-mail: syjung@skku.edu

BLDC motor with delta winding connection and designed it for automatic sun-roof driving motor employing the nonlinear Finite Element Method (FEM) for better accuracy. As mentioned above, BLDC motors with a delta winding connection need a slightly different approach in terms of both the designing process for the BEMF and phase current control compared with BLDC motor with wye winding connection and general AC type motor. After designing the motor, we analyzed the load characteristics according to the ideal current source analysis and 6-step voltage source analysis to identify the cause of the torque ripple. Moreover, a current controller which is a current regulator with PI controller was applied by Simulink, and a coupled analysis between BLDC motor with delta winding connection and the current controller was implemented to verify torque characteristic under real driving condition.

2. BLDC Motor with Delta Winding Connection

2.1. Governing Equation

For reference, the conventional BLDC motor voltage equation of one phase can be represented as the following equation,

$$V_a = R_s i_a + L_{aa}\frac{di_a}{dt} + L_{ab}\frac{di_b}{dt} + L_{ac}\frac{di_c}{dt} + e_a \quad (1)$$

where R_s represents the phase resistance, L_{aa} is the self-inductance, L_{ab} and L_{ac} are the mutual-inductances, and E_a indicates the BEMF of phase A.

The self-inductance and mutual-inductances can be replaced by the magnetizing-inductance and leakage-inductance as follow,

$$L_{aa} = L_{bb} = L_{cc} = L_{ls} + L_{ms} \quad (2)$$

$$L_{ab} = L_{ac} = L_{ba} = L_{bc} = L_{ca} = L_{cb} = -\frac{1}{2}L_{ms} \quad (3)$$

where L_{ls} is the leakage-inductance and L_{ms} is the magnetizing-inductance. By substituting the self-inductance and mutual-inductances for the leakage-inductance and magnetizing-inductance, the voltage equation is reformulated as follows.

$$V_a = R_s i_a + (L_{ls} + L_{ms})\frac{di_a}{dt} - \frac{1}{2}L_{ms}\left(\frac{di_b}{dt} + \frac{di_c}{dt}\right) + e_a \quad (4)$$

The sum of the three phase currents are zero, $i_a + i_b + i_c = 0$, therefore Eq. (4) can be changed to Eq. (5).

$$V_a = R_s i_a + \left(L_{ls} + \frac{3}{2}L_{ms}\right)\frac{di_a}{dt} + e_a \quad (5)$$

The second term of the right side, $(L_{ls} + 3/2L_{ms})$, can be referred as the synchronous inductance, L_s.

The output torque is calculated from the output power and the mechanical angular velocity.

$$P_{out} = e_a i_a + e_b i_b + e_c i_c \quad (6)$$

$$T^e = \frac{P_{out}}{\omega_m} = \frac{e_a i_a + e_b i_b + e_c i_c}{\omega_m} \quad (7)$$

2.2. Characteristics of BLDC Motor according to Winding Connection

The BLDC motor is classified in accordance with the stator winding connection method that is employed, wye or delta. Fig. 1 shows an equivalent circuit representing the whole system from the DC input to three-phase motor windings. Figs. 1(a) and (b) are for the wye and delta winding connections, respectively. The input source and switching part represented by a blue dotted line are identical for both the wye and delta winding connections. Only the three-phase load parts are different according to the winding arrangement, as shown by the red dotted line.

During a complete electrical cycle of 360°, the switching regions are divided into six different modes, modes 1 to 6 [9]. Each mode uses a different pair of switches. For example, mode 1 uses transistor 5 which is connected to phase C and transistor 6 which is connected to phase B. In this way, the six switches make up six modes at intervals of 60°. Fig. 2 shows the switching sequence and

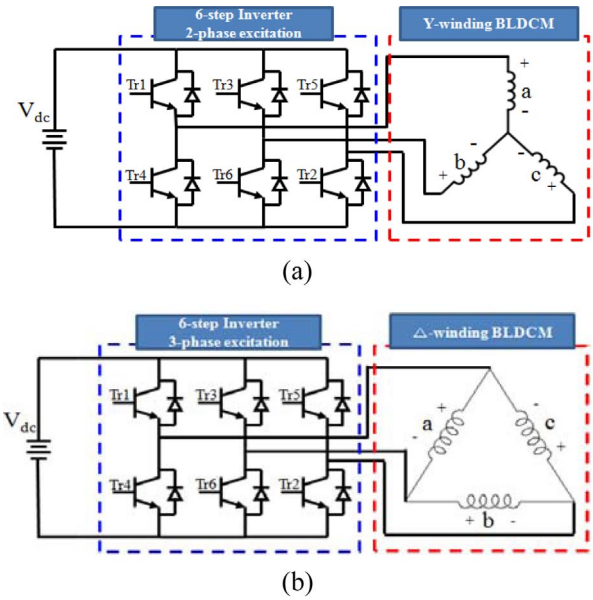

Fig. 1. (Color online) Equivalent circuit of BLDC motor according to winding connection: (a) Wye winding connection, two-phase excitation system, (b) Delta winding connection, three-phase excitation system.

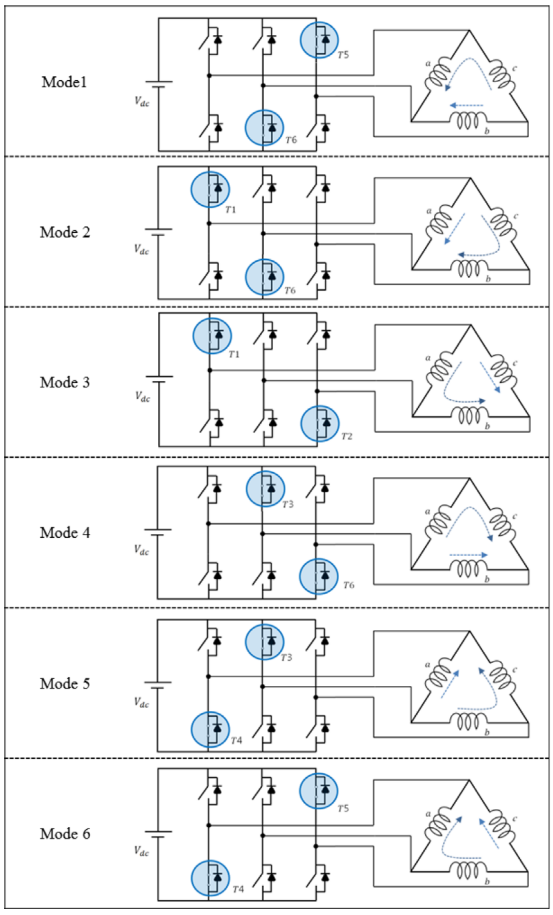

Fig. 2. (Color online) Switching sequence and current flows of three-phase delta winding connection.

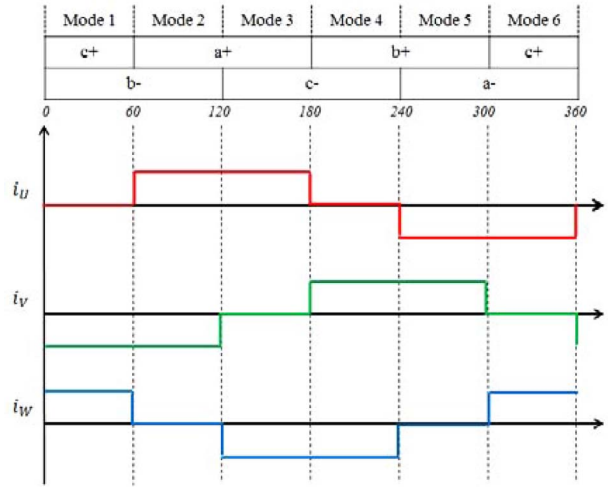

Fig. 3. (Color online) Motor input line current waveforms of winding connection methods, wye and delta.

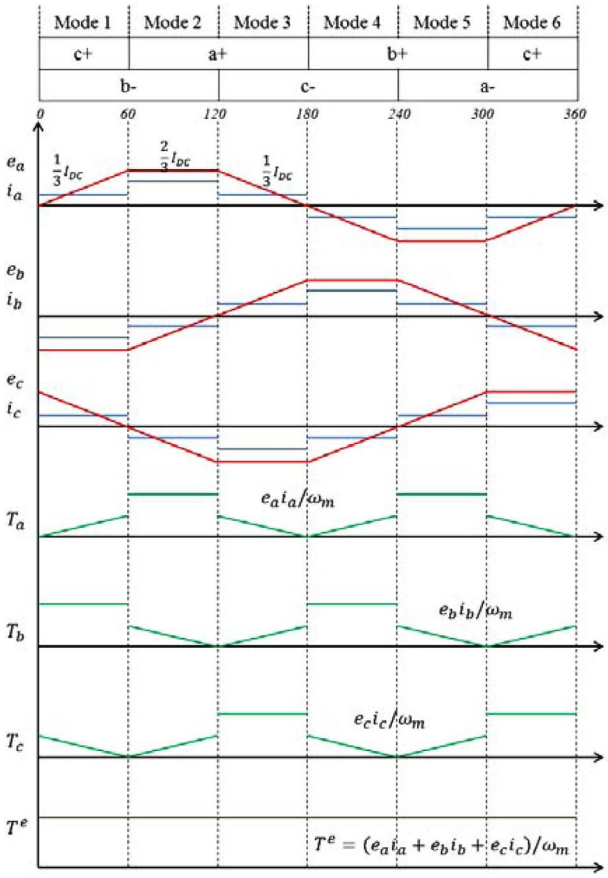

Fig. 4. (Color online) BEMF, phase current, and torque waveform of delta winding connection.

flow of the phase currents in the delta-winding connection.

When two out of six switches are turned on, only two phases are excited in the wye winding connection. Therefore, it can be called a two-phase excitation system. On the other hands, all three phases are excited in the delta winding connection method, as shown in Fig. 2, so we call it a three-phase excitation system.

Although the winding connection methods are different, the motor input line currents of the three phases have the same waveforms. This is represented in Fig. 3 and means that the switching sequence is equal in both cases regardless of the winding connection method.

In the ideal case, the BEMF of the BLDC motor with delta winding connection requires a 60° flat-top region, as mentioned before. According to the BEMF, the phase current has to be input in the form of a step function for constant torque production. Fig. 4 shows the BEMFs and phase current waveforms, which are necessary to drive a BLDC motor with delta winding connection, and the torque waveforms. As shown in Fig. 2, two phases are connected in series and are then connected with the other phase in parallel in each switching mode. For example, phases B and C are connected in series, and these phases are connected with phase A in parallel in mode 2. If we assume that the current at the input source, DC voltage

input, is I_{DC}, then $2/3I_{DC}$ flows into phase A and $1/3I_{DC}$ flows into phases B and C. The negative sign of the phase currents of B and C indicates that they flow in the opposite direction to the reference presented in Fig. 1.

2.3. Torque Ripple Occurrence according to Phase Commutation

At the phase commutation point, the currents of the three-phases are changed according to the switching sequence, as shown in Fig. 2. To clarify the occurrence of torque ripple, we consider the instance of phase commutation, from mode 2 to mode 3, as an example. The three-phase BEMFs are simplified as shown in Eq. (8). Then, they are assumed to be constant for phase commutation.

$$e_a = -e_c = E,\ e_b = 0 \tag{8}$$

The torque equation, given as Eq. (7), can be represented as a simple formulation as follow.

$$T^e = \frac{E(i_a - i_c)}{\omega_m} \tag{9}$$

From Eq. (9), it is confirmed that the output torque is directly proportional to the difference in current between phase A and phase C. In the ideal case, the currents of phases A and C and their difference are shown in Fig. 5. The difference between phases A and C is kept constant and there remains no torque ripple.

In a real situation, however, there exists a current delay due to the finite value of the inductance. Fig. 6 shows three different cases depending on the rising and falling speed of the current. If the rates of current increase and decrease are the same, the output torque is constant (Fig. 6(a)). In most cases, their rates are different though and this causes torque ripple (Figs. 6(b) & (c)). These differences in the switching current result from the coil inductance and potential difference between the DC link voltage and BEMF.

The torque ripple is the main factor generating noise or lowering the speed control characteristics. Therefore, many methods of removing torque ripple have been developed recently. In this study, we implemented a current controller for BLDC motor with delta winding connection and applied to the coupled analysis in order to examine and verify the causes of torque ripple characteristics in the current commutation region in detail.

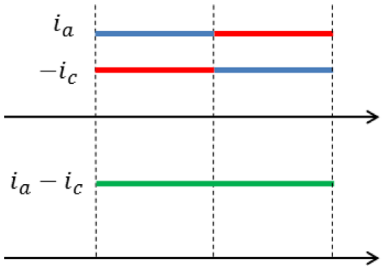

Fig. 5. (Color online) Current commutation in ideal case.

3. Simulation Results of Designed Model

3.1. Design specifications

In this paper, we deal with a BLDC motor used for driving an automobile sunroof, and its specifications are summarized in Table 1. According to these specifications, we designed the prototypes of BLDC motor of both the wye and delta winding connection type for the purpose of comparison through nonlinear FEM. Both models have identical stator with distributed winding arrangement. In addition, the notch has been chosen on teeth for reduction of torque ripple and cogging torque [10]. Furthermore,

Table 1. Specification of BLDC motor.

	Parameters	Spec.	Unit
Performance	Torque	0.104	Nm
	Speed	2,775	r/m
General	No. of Pole and Slot	4 / 12	
	No. of Phase	3	
	Air-Gap	0.5	mm
Stator	Outer Diameter	36	mm
Rotor	PM Property	Ferrite-9D	

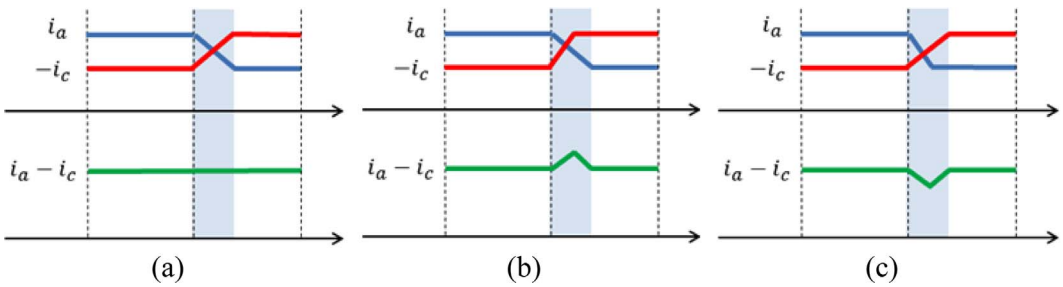

Fig. 6. (Color online) Form of currents causing torque ripple: (a) Constant torque, (b) Increased torque, (c) Decreased torque.

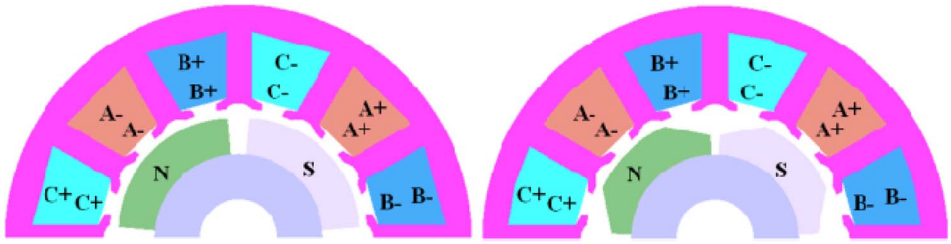

Fig. 7. (Color online) Designed BLDC motor with distributed winding: (a) Wye winding connection model, (b) Delta winding connection model.

Surface mounted Permanent Magnet (SPM) type has been sorted out for rotor with bread shaped and optimized permanent magnets to satisfy flat-top region of BEMF. For example, in the case of delta winding connection type model, 60° flat-top region of BEMF has been implemented through cut-off edge of permanent magnets. The design configurations for wye and delta winding connection models are shown in Fig. 7.

The BEMF waveform of delta winding connection, calculated by nonlinear FEM at the 4,550r/m operating point, is presented in Fig. 8. As mentioned above, the flat-top region of the BEMF waveform is maintained as close as possible to 60° for the delta winding connection, which is regarded as a final one for the sunroof driving motor.

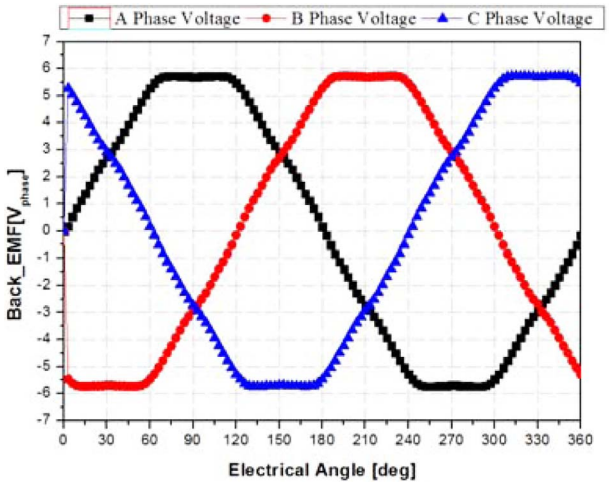

Fig. 8. (Color online) BEMF waveform of delta winding connection model.

3.2. Simulation Results of Ideal Current Source Analysis and 6-Step Voltage Source Analysis

Firstly, to identify the characteristics of the designed model, we conducted an ideal current source analysis. As explained before, it is assumed that the input current to each phase is ideal as the form of a step function shown in Fig. 4. Fig. 9 shows the line input current and phase input current, which is the rated current, satisfying the average torque. The operating point considered in this research is 2,775r/m and the average torque value is 0.104Nm. The calculated resistance and inductance are 0.381Ω and 0.367mH, respectively. The output torque waveform according to the input current is shown in Fig. 10. The torque ripple is 10.5%. The torque ripple occurs

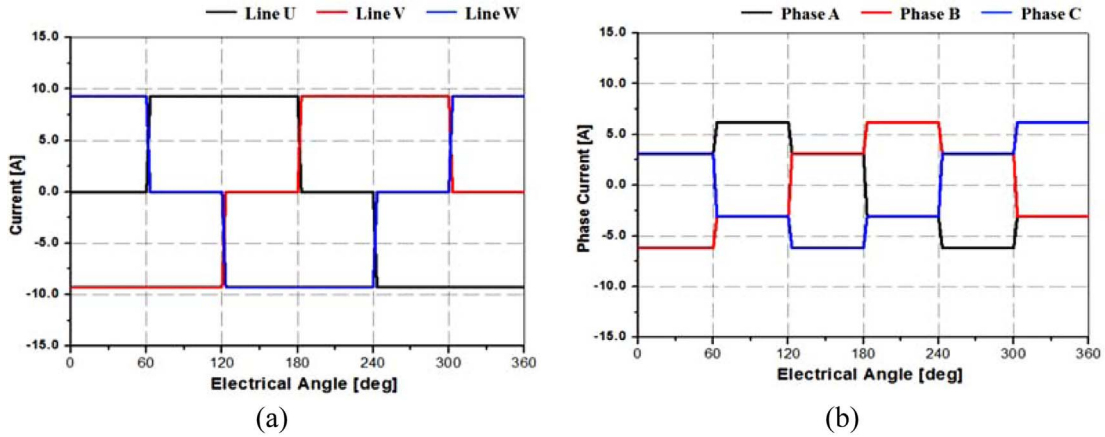

Fig. 9. (Color online) Motor input current in accordance with ideal current source analysis: (a) Line input current, (b) Phase input current.

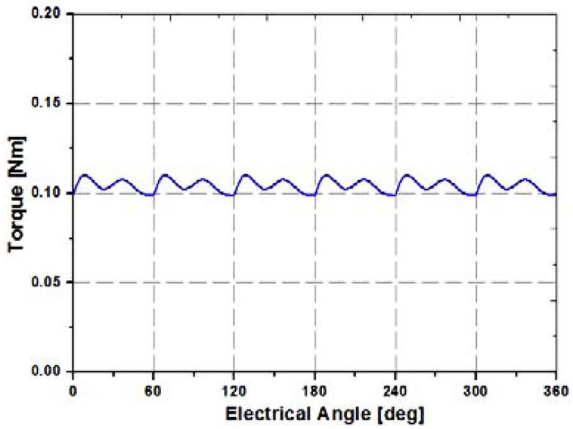

Fig. 10. (Color online) Output torque in accordance with ideal current source analysis.

due to the non-ideal BEMF, although the input current is ideal.

In real driving circumstances, however, the input current cannot increase and decrease rapidly because of the coil inductance [7]. Its speed is influenced by various factors, including the DC voltage and time constant. To determine the actual characteristics, we performed an additional 6-step voltage source analysis. In the 6-step voltage source analysis, the switching is changed every 60° during one electrical cycle, as shown in Fig. 2. The line input current and phase currents are shown in Fig. 11 and the analyzed output torque is represented in Fig. 12.

As explained, the current has a time delay when it increases (or decreases), and the discrepancy between the increase and decrease in speed gives rise to an increase in the torque ripple compared with the ideal current source analysis. In this case, the torque ripple stays 26.9%.

One drawback of the 6-step voltage source analysis is that it cannot control the DC input voltage. Its magnitude is determined automatically based on the current RMS magnitude. To achieve an average torque of 0.104Nm, the RMS magnitude of the input current is assigned the same value as that of the ideal current, which is $7.6A_{Line\_RMS}$. In this case, the required DC voltage magnitude is $7.0V_{DC}$. The rated voltage, however, is $9.0V_{DC}$. If the DC voltage is controlled and set to $9.0V_{DC}$, the average output torque would be more than 0.104Nm and the current varying speed would be changed. Therefore, it is necessary to analyze the designed model under the current controller using $9.0V_{DC}$ in order to investigate the real driving circumstances for better accuracy.

3.3. Current Regulator with PI Controller

We conducted the coupled analysis of the current controller and BLDC motor by means of Simulink [11]. When the current regulator takes account of the carrier wave without the PI controller, there are some demerits

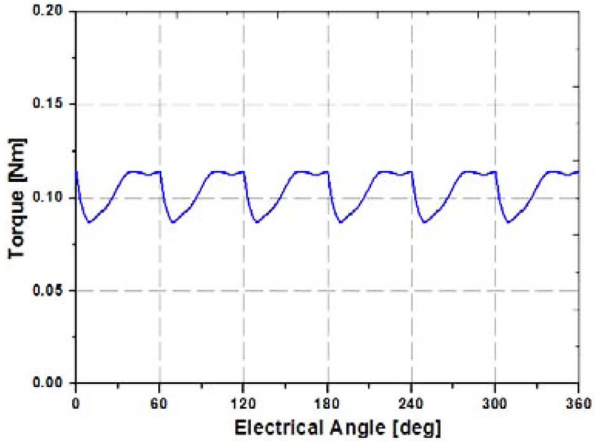

Fig. 12. (Color online) Output torque in accordance with 6-step voltage source analysis.

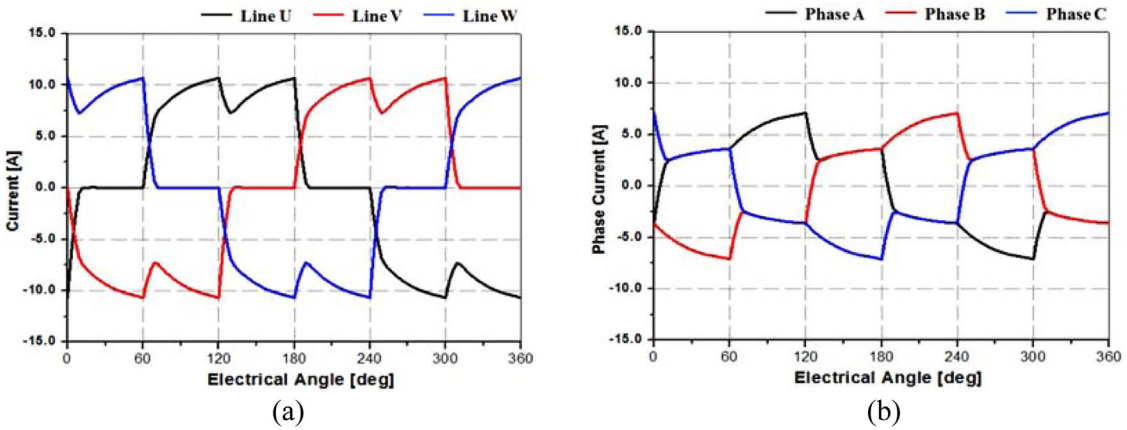

Fig. 11. (Color online) Motor input current in accordance with 6-step voltage source analysis: (a) Line input current, (b) Phase input current.

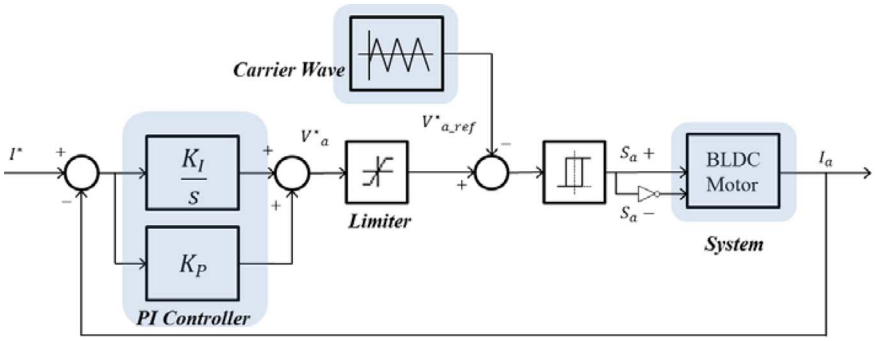

Fig. 13. (Color online) Current regulator with PI controller.

such as the current magnitude error and phase error, as compared with the reference current. Thus, we designed the current regulator with PI controller in order to overcome these problems. As shown in Fig. 13, which is a block diagram of the current controller considered in this study, it uses the PI controller as a compensator and triangular carrier wave. The gain of the PI controller is calculated based on Eq. (12) and Eq. (13).

$$K_I = R_s \times \omega_c \tag{12}$$

$$K_P = L_a \times \omega_c \tag{13}$$

According to the rotor position, a specific pair of switches, out of the six switches, should be turned on matching the BEMF with the current [12]. We considered the role of the BEMF in the detection of the rotor position. By generating the hall signal in accordance with the BEMF, we are able to determine the rotor position and make a decision regarding the switching sequence. The hall signal has a value of one when the BEMF is greater than zero, otherwise it has a value of zero, which is defined as zero-crossing as shown in Fig. 14. After that, each hall signal is multiplied by certain constants. In this controller, hall signal A from the phase A BEMF is multiplied by one, hall signal B from the phase B BEMF is multiplied by two, and hall signal C from the phase C BEMF is multiplied by four. Then, by summing these three values, the six different region numbers are obtained, corresponding to the six modes.

In Fig. 15, the BLDC motor part representing the three-phase load is simply expressed as the equivalent circuit of the delta winding connection, including the phase resistance, inductance, and the BEMF. The numerical result of the BEMF obtained through nonlinear FEM is applied to the BEMF voltage source in the form of a look-up table, in order to consider the characteristics of the designed model in detail. The output torque is calculated with the phase current and BEMF making use of Eq. (7).

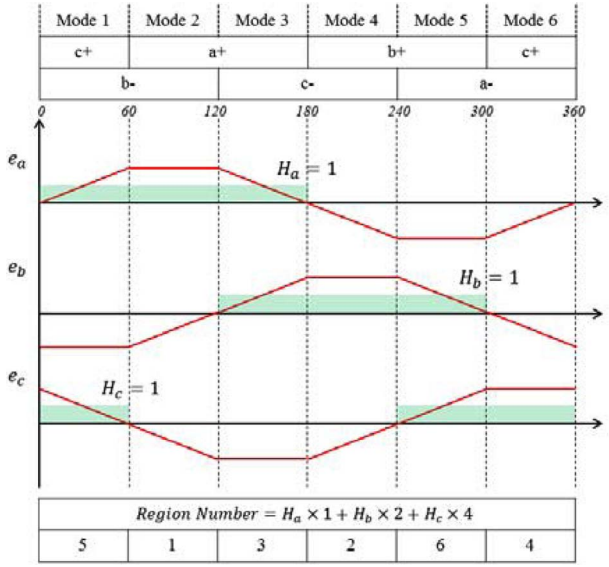

Fig. 14. (Color online) BEMF zero crossing and generation region number.

3.4. Simulation Result of Designed Model with Current Controller by Simulink

Through the coupled analysis of the current controller and designed model, the input current waveforms in terms

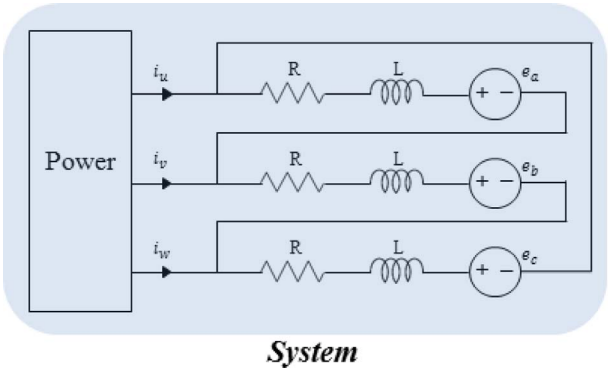

Fig. 15. (Color online) Equivalent circuit of delta winding connection.

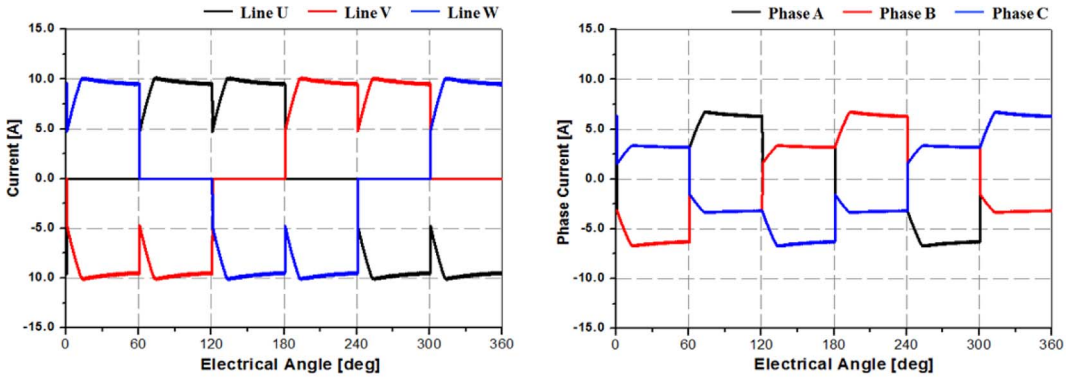

Fig. 16. (Color online) Motor input current in accordance with coupled analysis of current controller and BLDC motor: (a) Line input current, (b) Phase input current.

of the line and phase are shown in Fig. 16. In contrast to the 6-step voltage source analysis, a DC voltage of $9.0V_{DC}$ is applied, which is the rated voltage. This affects the input current rising and falling time such that their speeds are increased. The required line current of the 6-step voltage source analysis is $10.7A_{pk}$ and it increases to a peak value at 0.002sec from the zero crossing point of the phase A BEMF, while the required line current of the coupled analysis is $10.2A_{pk}$ and it increases to a peak value at 0.000545sec under the same conditions.

The output torque of the coupled analysis is shown in Fig. 17. In this case, the torque ripple is 57.0%. There exists additional torque ripple compared with the 6-step voltage source analysis result, besides the torque ripple due to the current commutation mentioned above.

To clarify the cause of this additional torque ripple, the input phase current, BEMF, and phase torque are shown in Fig. 18 at the 120° point in the electrical angle, which is the moment of current commutation from mode 2 to mode 3. The input current of phase A is supposed ideally to vary from $2/3I_{DC}$ to $1/3I_{DC}$. With the current controller,

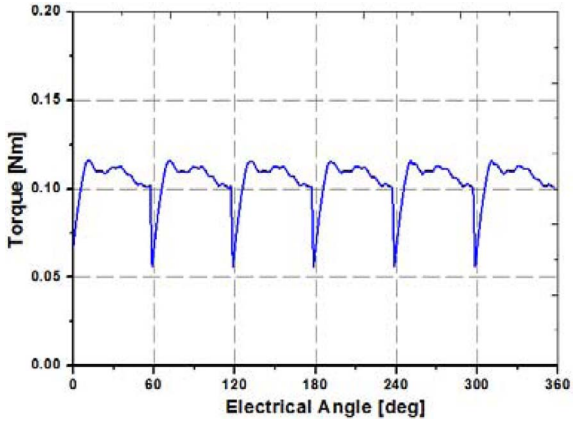

Fig. 17. (Color online) Output torque in accordance with coupled analysis of current controller and BLDC motor.

however, it is identified that the phase current decreases to a lower point than expected. As a result, it influences on the torque ripple increases.

If we consider all of the phases in detail, only the magnitudes of the currents of phases A and C are

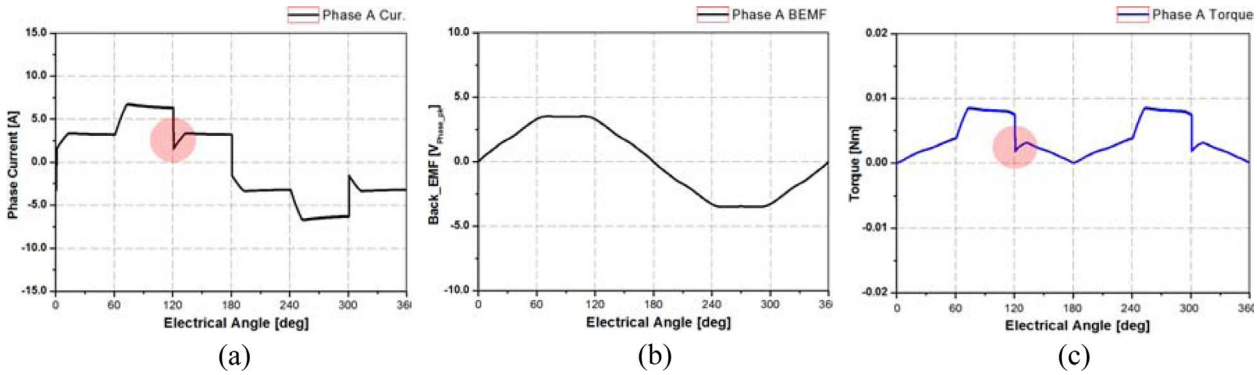

Fig. 18. (Color online) Coupled analysis results in terms of phase A: (a) Input current of phase A, (b) BEMF of phase A, (c) Torque of phase A.

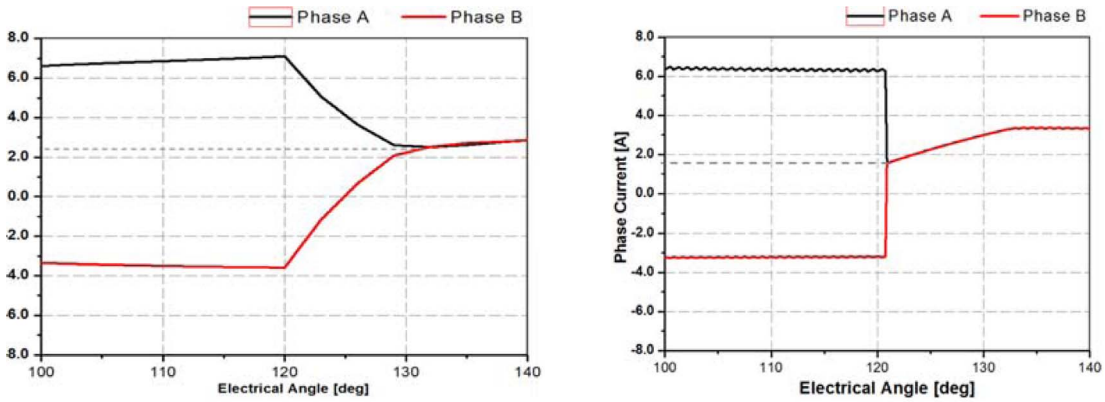

Fig. 19. (Color online) Comparison results of phase input current at the point of current commutation: (a) 6-step voltage source analysis, (b) Coupled analysis with current controller.

changed, while both the magnitude and direction of the current of phase B are changed at the same time. Moreover, immediately after mode 3 began, an identical current whose magnitude is $1/3I_{DC}$ flows into phases A and B, since they are connected in series. In other words, as the current of phase A is changed from $2/3I_{DC}$ to $1/3I_{DC}$, that of phase B changes from $-1/3I_{DC}$ to $1/3I_{DC}$ in order to maintain an identical value. Thus, a falling current of phase A and a rising current of phase B are encountered at a specific point depending on their rising and falling speeds and then they reach $1/3I_{DC}$. In particular, it is found that the 6-step voltage source analysis and coupled analysis give different results for this meeting point owing to the different input voltages and switching frequencies [13]. The expanded graph of the phase currents corresponding to both analysis methods is represented in Fig. 19. In the case of the 6-step voltage analysis, the phase A and B currents meet each other at the 2.5A point, while in the case of the coupled analysis, they encounter each other at the 1.5A point. This current gap between the meeting points causes an increase in the torque ripple from 26.9% to 57.0%. Therefore, it is confirmed that a specific and optimized current controller is necessary to improve the torque characteristics of the BLDC motor with delta winding connection.

In Table 2, all of the results corresponding to the three different analysis methods are summarized.

Table 2. Analysis results in accordance with three different methods

	Ideal Current Source Analysis	6-step Voltage Analysis	Controller Analysis
Line Current	9.3 A_{pk}	10.7 A_{pk}	10.2 A_{pk}
Phase Current	6.2 A_{pk}	7.1 A_{pk}	6.8 A_{pk}
Ave. Torque		0.104 Nm	
Torque Ripple	10.5%	26.9%	57.0%

4. Summary

In this study, we designed a BLDC motor with delta winding connection based on nonlinear FEM. In order to compare the torque ripple characteristics, we performed both an ideal current source analysis and 6-step voltage source analysis. The coil inductance influences the torque ripple, since the rates of increase and decrease of the current are different. Therefore, the torque ripple of the ideal current source analysis, 10.5%, is increased to 26.9% when the 6-step voltage analysis is applied. In the 6-step voltage source analysis, however, it is impossible to make the input DC voltage be equal to the rated value. For this reason, the current controller is required. To verify an effect of the rated voltage as well as a coupled analysis between the controller and BLDC motor, we designed the current regulator with PI controller corresponding to the delta winding connection. As a result, the torque ripple is increased to 57.0%. Finally, through the comparison of the results, the reason for the torque ripple in the delta winding arrangement of the BLDC motor has been investigated thoroughly.

Acknowledgements

This work was supported by the Human Resources Development program (No. 20134010200550) and the Energy Efficiency & Resources Core Technology Program (No. 20142010102970) of the Korea Institute of Energy Technology Evaluation and Planning (KETEP), granted

financial resource from the Ministry of Trade, Industry & Energy, Republic of Korea.

References

[1] C. Bi, Z. J. Liu, and S. X. Chen, IEEE Trans. Magn. **36**, 697 (2000).
[2] Jibin Zou, Wenjuan Qi, Yongxiang Xu, Fei Xu, Yong Li, and Jianjun Li, IEEE Trans. Magn. **48**, 4220 (2012).
[3] Jin-Woo Jung and Tae Heoung Kim, J. Magn. **15**, 40 (2010).
[4] Hong-seok Kim, Yong-Min You, and Byung-Il Kwon, IEEE Trans. Magn. **49**, 2193 (2013).
[5] Sun-Kwon Lee, Gyu-Hong Kang, Jin Hur, and Byoung-Woo Kim, IEEE Trans. Magn. **48**, 4662 (2012).
[6] Jiang Xintong, Xing Jingwei, Li Yong, and Lu Yongping, IEEE Trans. Magn. **45**, 4601 (2009).
[7] P. Pillay and R. Krishnan, IEEE Trans. Ind. Appl. **25**, 274 (1989).
[8] J. R. Hendershot and T. J. E. Miller, Design of brushless permanent-magnet machines, Motor Design Books LLC. Florida (2010) pp. 273-305.
[9] D. Lin, P. Zhou, and Z. J. Cendes, IEEE. Trans. Magn. **45**, 5383 (2009).
[10] S. Wang and J. Kang, IEEE Trans. Magn. **36**, 1119 (2000).
[11] Jaehyuck Kim, Yong-hoe Jeong, Yong-Hee Kang, Seunghun Lee, and Jang-Yeop Park, J. Magn. **19**, 282 (2014).
[12] Keunsoo Ha, Jaehyuck Kim, and Jang Young Choi, J. Magn. **19**, 90 (2014).
[13] Hyun-Soo, Kang, Byoung-Kuk Lee, and Tae Heoung Kim, J. Magn. **18**, 50 (2013).